TWO-RAY CHANNEL MODELS WITH DOPPLER EFFECTS FOR LEO SATELLITE COMMUNICATIONS

Weimin Zhang

Wireless Communications, Information Science Division, Defence Science and Technology Group,
Third Avenue, Edinburgh, SA 5111, Australia

Email: weimin.zhang@defence.gov.au

Abstract – *In this paper we present some two-ray models with Doppler effects for Low Earth Orbit (LEO) satellite links. We show that satellite motion-caused Doppler shifts are different along the two rays, resulting in a time-varying phase shift. This is quantified with a few Doppler models and approximations. The combined interference effects, along with the path length difference caused phase shift, are calculated using a generic LEO pass-over. Channel gains are computed and compared using various antenna patterns and system parameters. The models show good agreements except for very low elevation angles. They demonstrate that a tracking antenna is effective in reducing fading for moderate to high elevation angles. Fixed patch antennas perform well. Omnidirectional and dipole antennas perform poorly. Higher carrier frequency and higher antenna height lead to faster fades. The fading becomes deeper at low elevation angles. Very fast fading is observed near the ends of a pass-over.*

Keywords – Curved Earth two-ray, ground reflection, LEO channel model, LEO satellite channel, satellite Doppler, two-ray Doppler channels

1. INTRODUCTION

A LEO satellite-Earth channel model usually consists of a Line-Of-Sight (LOS) component and a multipath component. It may be modelled statistically by a 2D impulse response over the Doppler-delay domain [1] [2] [3]. The distribution is environment dependent. For large data it may follow a Rician distribution at high elevation angles and Rayleigh or lognormal distributions at low elevations. During a satellite pass-over, the channel is non-stationary and may be modelled by a state machine of distributions [3]. For a moving earth terminal, the Doppler spectrum may be modelled by a Jakes-shaped Rayleigh process [4]. In this paper we assume a fixed ground terminal.

Sometimes, a LEO satellite channel can be simply modelled by a deterministic model, such as a LOS model or line-tracing model [5]. When the ground terminal is at an open field or water surface, it fits the two-ray scenario. A two-ray model is the first step up from LOS and enters the multipath arena. It may help us understand multipath interference-caused fading. As a deterministic model it may be more convenient for engineering design, e.g. antenna selection.

A classical two-ray channel [6] [7] [8] is for stationary or slow-motion radios [9] where the Doppler effect is negligible. The assumption is that there is no frequency change between the two rays.

The phase and amplitude differences are solely caused by the different path lengths. The wave interference leads to level fluctuations at the receiver. A two-ray model appears in ITU Recommendations [10] where typical surface parameters are specified.

For a LEO satellite earth link, the fast movement of the satellite breaks the fixed frequency assumption. The Doppler shifts along the two rays are different due to the non-zero angle between them. Although the angle and frequency shift are small, the accumulate phase shift may be significant. It is in addition to the phase shift caused by path length difference, which results in a different amplitude fluctuation or fading. The discussion of this phenomenon has not been found in the literature, nor is the application of two-ray model for LEO-ground links.

A simplistic LEO two-ray model may use a series of isolated static episodes at each time instance. It will lead to an unrealistic amplitude fading pattern, reducing the fidelity of the model and its validity. The correct way is to incorporate the Doppler shift effects in the model itself. This is the motivation and goal of the investigation.

It is also curious to see how the channel response changes when the ground antenna pattern and other system parameters are changed, including antenna height, carrier frequency, distance, satellite orbit, surface properties and wave polarization.

To achieve the aims we will base our analysis on one LEO pass-over and calculate the channel gains using different Doppler models [11] [12]. The convergence of the results will serve as cross-checks and validation for all our models.

The main contributions of the paper are

(1) Introduce Doppler effects to the two-ray channel model for LEO satellite links.

(2) Explore different Doppler shift models and algorithms and the results agree well except for very low elevations.

(3) Compare antennas and system parameters on their channel responses.

The method of adding Doppler shifts may also be of use to multi-ray and line-tracing modelling.

In the rest of the paper, we first review and introduce three ingredients of our models: the classic two-ray model on a curved earth, a typical LEO satellite pass-over with specified orbit and distances, and the Doppler modelling methods especially for the reflected links. We derive our channel gains according to the Doppler models and discuss numerical methods. Then we model a selection of example scenarios with real and artificial antenna patterns and system parameters and compare the results.

2. CURVED EARTH TWO-RAY MODEL

2.1 Static two-ray geometry

A 2D curved earth two-ray geometry assumes a smooth and uniform terrain, as illustrated in Fig. 1. The flat earth model is inaccurate for our long-distance scenarios.

If the positions of satellite A and the ground terminal B are known, the reflect point C is fully determined. However, unlike the flat earth model, it cannot be expressed explicitly. A numerical solution is required.

To construct the implicit equation, we use the equal relationship of the two grazing angles [13] in Fig. 1.

$$\alpha = \alpha_1 = \alpha_2 \qquad (1)$$

From the two triangles OACO and OCBO we have

$$\alpha_1 = \cos^{-1} \frac{H_1 \sin(d_1 / R_E)}{\sqrt{H_1^2 + R_E^2 - 2H_1 R_E \cos(d_1/R_E)}} \qquad (2)$$

$$\alpha_2 = \cos^{-1} \frac{H_2 \sin(d_2 / R_E)}{\sqrt{H_2^2 + R_E^2 - 2H_2 R_E \cos(d_2/R_E)}} \qquad (3)$$

where $H_1 = h_1 + R_E$ and $H_2 = h_2 + R_E$.

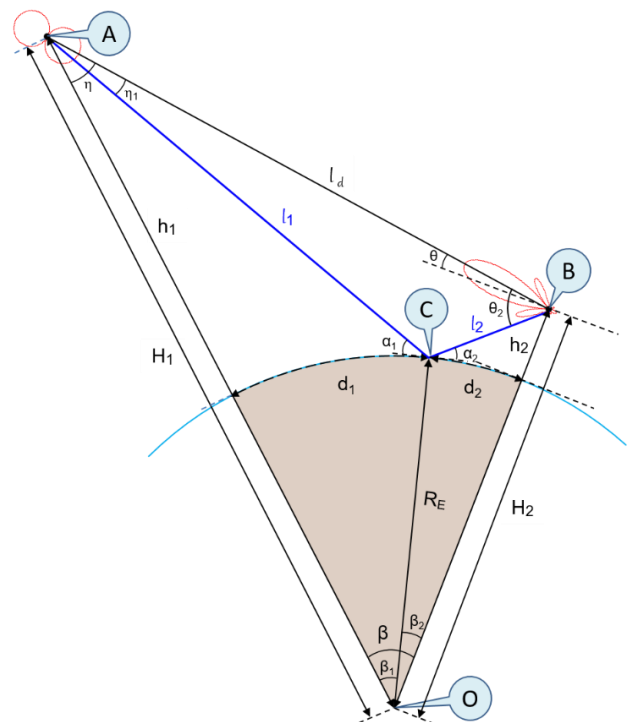The given surface distance is

$$d_s = d_1 + d_2. \qquad (4)$$

Fig. 1 - Curved earth two-ray geometry

When substituting (2)-(4) into (1) we can define a function

$$q(d_1) = \frac{H_1 \sin(d_1 / R_E)}{\sqrt{H_1^2 + R_E^2 - 2H_1 R_E \cos(d_1/R_E)}} - \frac{H_2 \sin((d_s - d_1) / R_E)}{\sqrt{H_2^2 + R_E^2 - 2H_2 R_E \cos((d_s - d_1)/R_E)}} \qquad (5)$$

Then d_1 can be solved from $q(d_1) = 0$ numerically. If using MATLAB, variable precision algorithm (vpa) solver *vpasolve* must be used, as double precision solvers *fzero* and *solve* result in unacceptable errors.

From the triangle OABO, the earth center angle $\beta = \frac{d_s}{R_E}$. The length of the direct range is

$$l_d = \sqrt{H_1^2 + H_2^2 - 2H_1 H_2 \cos \beta} \qquad (6)$$

The elevation angle is

$$\theta = \sin^{-1} \frac{H_1^2 - H_2^2 - l_d^2}{2 H_2 l_d} \qquad (7)$$

Once d_1 is known, all other parameters d_2, β_1, β_2 can be calculated, e.g. $\beta_1 = \frac{d_1}{R_E}$. The range sections are

$$l_1 = \sqrt{H_1^2 + R_E^2 - 2 H_1 R_E \cos \beta_1} \qquad (8)$$

$$l_2 = \sqrt{H_2^2 + R_E^2 - 2 H_2 R_E \cos \beta_2} \qquad (9)$$

For a satellite or ground antenna, the angle between the two rays is known as the 'two-ray angle'. The two-ray angle at the satellite is

$$\eta_1 = \cos^{-1} \frac{l_d^2 + l_1^2 - l_2^2}{2 \, l_d \, l_1} \qquad (10)$$

For a typical LEO with $h_2 \leq 18$ m, the angle $\eta_1 < 2.3 \times 10^{-3}$ degree and the antenna gains are effectively equal for the two rays, equivalent to using an omnidirectional antenna.

However, the situation is very different for the ground antenna. The two-ray angle for the ground antenna is

$$\theta_2 = \cos^{-1} \frac{l_d^2 + l_2^2 - l_1^2}{2 \, l_d \, l_2} \qquad (11)$$

It changes vastly so that the antenna pattern plays an important role. The ground antenna shown in Fig. 1 is a tracking antenna, with its maximum gain facing the satellite. Fixed antennas will also be used in our analysis.

2.2   Classic two-ray channel model

In a classic two-ray model the radios involved are static. The direct ray and the earth-reflected ray meet at the receiver with the same frequency. Due to the different path lengths, there is a carrier phase shift between the two rays as

$$\Phi_{2R} = \frac{2\pi f_0 (l_1 + l_2)}{c} + \varphi_\rho - \frac{2\pi f_0 l_d}{c} \qquad (12)$$

The first term is the carrier and phase of the reflected ray, φ_ρ is the phase of the surface reflect coefficient $\rho = |\rho| \exp i\varphi_\rho$, the third term is the carrier and phase of the direct ray, f_0 is the carrier frequency in Hz and c is the speed of light. The Carrier Wave (CW) response is

$$g_{2R} = \frac{c}{4\pi f_0} \left(\frac{g_1(0) g_2(\vartheta_d)}{l_d} + \frac{|\rho| g_1(\psi_1) g_2(\vartheta_r) e^{i\Phi_{2R}}}{l_1 + l_2} \right) \qquad (13)$$

where $g_1(\vartheta)$ and $g_2(\vartheta)$ are the satellite/ground antenna voltage gains versus the deviation angle ϑ. The ϑ is defined in the vertical plane containing the earth center, the satellite and the ground terminal (Fig. 1). The reference of ϑ is defined as follows. For a tracking antenna, when $\vartheta = 0$, its gain reaches the maximum. For a tracking ground antenna, $\vartheta_d = 0$ and $\vartheta_r = \theta_2$ (see Fig. 1). For a fixed ground antenna, the reference angle $\vartheta = 0$ points to the horizon. $\vartheta_d = \theta$ is the elevation angle, and $\vartheta_r = \theta - \theta_2$. For a tracking satellite antenna, since η_1 is tiny, $g_1(\eta_1) \approx g_1(0)$. If it is a tracking or isotropic satellite antenna, the above equation can be simplified to

$$g_{2R} = \frac{c g_1(0)}{4\pi f_0} \left(\frac{g_2(0)}{l_d} + \frac{|\rho| g_2(\theta_2) e^{i\Phi_{2R}}}{l_1 + l_2} \right) \qquad (14)$$

The reflection coefficient ρ is a function of grazing angle α, frequency f_0, ground relative dielectric constant ε_r, surface conductivity σ, and the polarization of the wave [13] [14].

For horizontally polarized waves the reflection coefficient is

$$\begin{aligned} \rho_h &= \rho_h(\alpha, f_0, \varepsilon_r, \sigma) \\ &= \frac{\sin \alpha - \sqrt{(\varepsilon_r - i\chi) - \cos^2 \alpha}}{\sin \alpha + \sqrt{(\varepsilon_r - i\chi) - \cos^2 \alpha}} \end{aligned} \qquad (15)$$

where

$$\chi = \frac{\sigma}{2\pi f_0 \varepsilon_0} \qquad (16)$$

and $\varepsilon_0 = 8.854187817 \times 10^{-12} \, A^2 s^4 kg^{-1} m^{-3}$ is the electric constant or dielectric constant in vacuum.

The 'horizontal' means E-field is perpendicular to the plane of incidence, and '$h = \perp$' [7] [6].

The 'vertically' polarized wave means the E-field is parallel to the plane of incidence, '$v = \parallel$' [6].

$$\begin{aligned} \rho_v &= \rho_v(\alpha, f_0, \varepsilon_r, \sigma) \\ &= \frac{(\varepsilon_r - i\chi) \sin \alpha - \sqrt{(\varepsilon_r - i\chi) - \cos^2 \alpha}}{(\varepsilon_r - i\chi) \sin \alpha + \sqrt{(\varepsilon_r - i\chi) - \cos^2 \alpha}} \end{aligned} \qquad (17)$$

For circular and elliptical polarized waves, the ρ and g_{2R} may be derived from a combination of the above.

The decibel gain is

$$G_{2R} = 20 \log_{10} |g_{2R}| \qquad (18)$$

3. A SIMPLE LEO GEOMETRY

A simple generic LEO satellite geometry is introduced as shown in Fig. 2. Two parameters h_1 and d can fully define the system, where h_1 is the Satellite (SAT) altitude, and d is the surface distance between the Ground Terminal (GT) and the sub-SAT track. For simplicity, a zero-inclination orbit is chosen so that the sub-SAT track is on the equator (red dashed line). The ground terminal is at zero longitude. Compared with a specific LEO orbit there may be a small discrepancy, depending on the inclination.
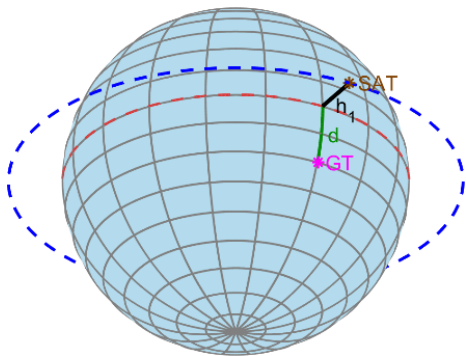
Fig. 2 – A simple LEO satellite geometry specified by two parameters, (h_1, d). The blue dashed line is the satellite orbit, where the SAT is shown at the $\xi = 0$ longitude. The red dashed line is the sub-SAT track. It is drawn to scale, $h_1 = 2000$ km, $d = 2224$ km.

The calculation is based on one satellite pass-over with different parameters.

We use a spherical coordinate (r, ψ, ξ) centered at the earth center, where r, ψ, and ξ are radius, latitude and longitude respectively. The ground terminal is located at $(H_2, \psi_G, 0)$, where $H_2 = h_2 + R_E$ is the radius of the GT antenna, and ψ_G is its latitude.

$$\psi_G = d/R_E \qquad (19)$$

For most applications the ground antenna height $h_2 > 0$ so that there is a ground reflection. Even when h_2 is small, e.g. 0.5 m, it still needs to be specified by the model. Otherwise, if $h_2 = 0$ it will become a LOS model.

The position of the LEO satellite is $(H_1, 0, \xi(t))$ and the time $t \in [t_{\min}, t_{\max}]$. Its time-varying longitude is

$$\xi(t) = 2\pi t / T_{sat} \qquad (20)$$

where T_{sat} is the period of the satellite orbit, and

$$T_{sat} = 2\pi \sqrt{H_1^3 / \mu_G} \qquad (21)$$

where μ_G is the geocentric gravitational constant [6] and $\mu_G = 3.986004418 \times 10^{14} m^3 s^{-2}$.

The direct range $l_d(t)$ between the satellite and the ground terminal is

$$l_d(t) = \sqrt{H_1^2 + H_2^2 - 2H_1 H_2 \cos\psi_G \cos\xi(t)} \qquad (22)$$

The elevation angle viewed from the ground terminal towards the satellite is [2]

$$\theta(t) = \tan^{-1} \frac{\cos\psi_G \cos\xi(t) - H_2/H_1}{\sqrt{1 - \cos^2\psi_G \cos^2\xi(t)}} \qquad (23)$$

Note this formula is for satellites with zero-degree inclination, including geostationary satellites. The earth's self-rotation, up to about 6% of LEO velocity, is not taken into consideration. If both are considered, the error may be smaller due to a partial cancellation.

The minimum elevation is determined by the GT antenna height h_2 or H_2 as

$$\theta_{min} = \sin^{-1} R_E/H_2 - \pi/2 \qquad (24)$$

which may not be calculated with $\cos^{-1}(\cdot)$ due to ambiguity. The maximum elevation happens when the satellite is at $\xi(0) = 0$ as

$$\theta_{max} = \tan^{-1} \frac{\cos\psi_G - H_2/H_1}{\sqrt{1 - \cos^2\psi_G}} \qquad (25)$$

At any given time t, the SAT's earth center angle is

$$\beta(t) = \sin^{-1}(l_d(t) \cos\theta(t)/H_1) \qquad (26)$$

The earth surface distance from SAT to GT is

$$d_s(t) = R_E \beta(t) \qquad (27)$$

The azimuth angle $\omega_a(t)$ is the angle between the $\xi = 0$ plane and the earth center plane containing both GT and SAT. From the surface right-angle triangle, it is

$$\omega_a(t) = \cot^{-1}(\cot\xi(t) \sin\psi_G) \qquad (28)$$

The range rate (radial velocity) of the direct path can be derived analytically from (22) as

$$v_d(t) = \frac{dl_d(t)}{dt}$$
$$= \frac{2\pi H_1 H_2 \cos\psi_G \sin(\xi(t))}{T_{sat}\sqrt{H_1^2 + H_2^2 - 2H_1 H_2 \cos\psi_G \cos(\xi(t))}} \qquad (29)$$

For fixed ground terminal, $v_d(t)$ is the speed projected on the direct link l_d due to SAT movement.

Unfortunately for the reflected path there is no closed-form expression, so that $v_r(t)$ has to be calculated numerically.

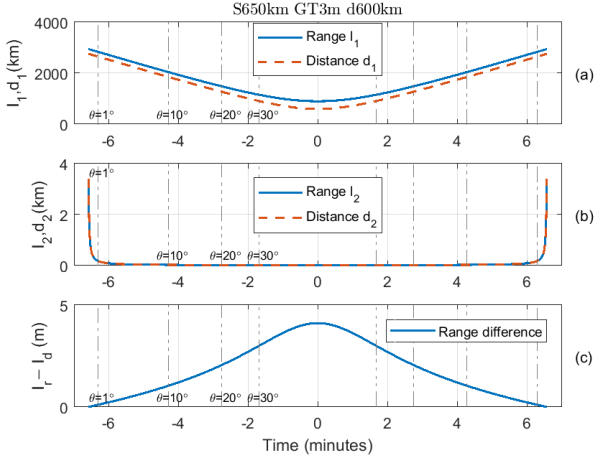Some example ranges, distances and angles are plotted in Fig. 3 to Fig. 5.

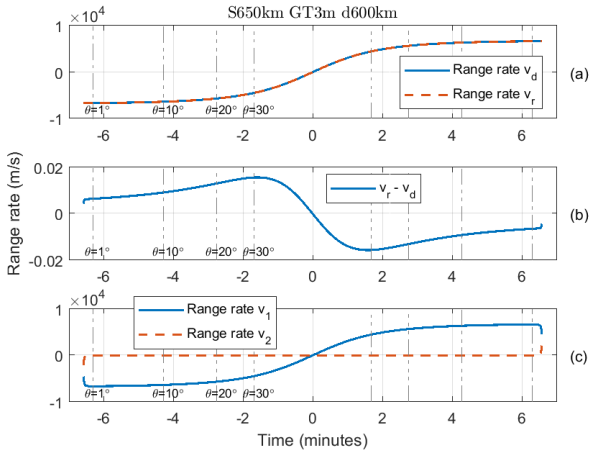**Fig. 3** – Range and distance examples with elevation angles θ.
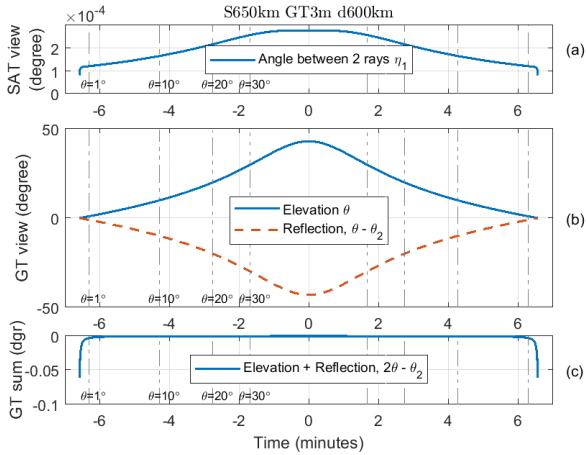

Fig. 4 – Example range rates and range rate difference.

Fig. 5 – Example satellite and ground terminal ray angles.

4. MODELLING OF DOPPLER SHIFT

We need to model the Doppler shift of the direct link and the reflected link. There are different Doppler models and approximations, as the modelling of Doppler effects is possibly still an open problem [15].

4.1 Doppler shift by nodes' motions

For the direct link in its 1D space (straight line), the received frequency is given [15] as

$$f_R(t) = f_0 \frac{1 - v_R(t)/c}{1 + v_S(t)/c} \qquad (30)$$

where f_0 is the source frequency, $v_R(t)$ is the velocity of the receiver, $v_S(t)$ is the velocity of the source, and c is the speed of propagation, or speed of light here.

In this definition the movements of the source and the receiver have different contributions, although the difference is small, as $v_R, v_S \ll c$.

If the ends or nodes move in an arbitrary direction, the Doppler is related to the projected velocities to the 1D link towards each other.

In Fig. 6 a generic two-ray Doppler model is illustrated with the projected moving ends. Satellite A moves with velocity $\vec{V}_A(t)$. The ground terminal moves with $\vec{V}_B(t)$. These movements cause reflection point C to move with $\vec{V}_C(t)$. Only those projected velocities along the edges of the triangle ABCA are relevant. The plane containing the triangle is also moving. However, it is convenient to assume it is fixed with the media.
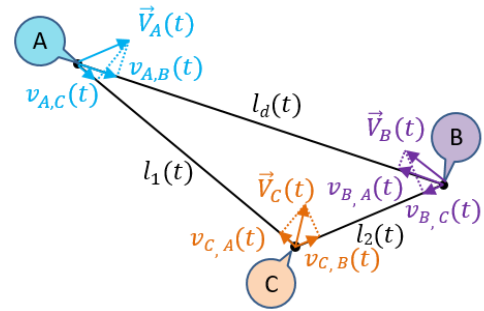

Fig. 6 – Node velocities projected on links, a general model.

When the nodes move there are six velocities projected on the edges linking A, B and C. We denote the velocity of X relative to Y as $v_{X,Y}$ and have colour coded the 3D velocities and their projected velocities on the links. For example, for A, its velocity $\vec{V}_A(t)$ projected on the link l_d towards B is $v_{A,B}(t)$. A positive velocity is when the link distance increases (opposite to the component vector

though), so that it produces a negative Doppler shift. The reflector C moves passively and its projected velocity along l_1 away from A is $v_{C,A}$, and along l_2 away from B is $v_{C,B}$.

When a carrier frequency f_0 is transmitted from A, the received frequency at B via the direct link is $f_{B,A}(t)$

$$f_{B,A}(t) = f_0 \frac{1 - v_{B,A}(t)/c}{1 + v_{A,B}(t)/c}. \qquad (31)$$

In the opposite direction, when a CW of f_0 Hz is transmitted from B, the received frequency at A is

$$f_{A,B}(t) = f_0 \frac{1 - v_{A,B}(t)/c}{1 + v_{B,A}(t)/c}. \qquad (32)$$

Obviously, $f_{A,B}(t) \neq f_{B,A}(t)$, although they are very similar when the velocities are far less than c.

For the reflected ray, one way is to calculate it section by section before cascading them [11]. The frequency at C from A is

$$f_{C,A}(t) = f_0 \frac{1 - v_{C,A}(t)/c}{1 + v_{A,C}(t)/c}. \qquad (33)$$

The frequency at B is

$$\begin{aligned} f_{B,CA}(t) &= f_{C,A}(t) \frac{1 - v_{B,C}(t)/c}{1 + v_{C,B}(t)/c} \\ &= f_0 \frac{c - v_{C,A}(t)}{c + v_{A,C}(t)} \cdot \frac{c - v_{B,C}(t)}{c + v_{C,B}(t)} \end{aligned} \qquad (34)$$

In the opposite direction B→C→A, assume f_0 is transmitted from B, the received frequency at A is

$$f_{A,CB}(t) = f_0 \frac{c - v_{A,C}(t)}{c + v_{C,A}(t)} \cdot \frac{c - v_{C,B}(t)}{c + v_{B,C}(t)} \qquad (35)$$

The calculations in (34) and (35) treated the reflected signal as a new source [11]. An alternative model is to treat the reflected path as a whole or known as the spatial mirror method [12]. It will be presented with the range rate approximation next.

4.2 Doppler shift by range rates

The calculations above require individual node positions in the 3D space, before being projected to each link. The efforts appear to be not well rewarded.

A simpler approximation is based on the range rate

$$v(t) = \frac{dl(t)}{dt} \approx \frac{l(t) - l(t - \Delta t)}{\Delta t} \qquad (36)$$

where Δt is the time increment between range samples. There are only three link-based range rates, as illustrated in Fig. 7.
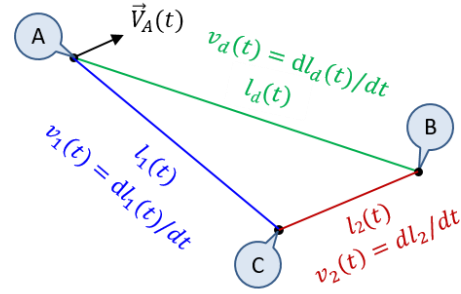

Fig. 7 – Range rates of each section.

The direct link. The range rate of the direct link is

$$v_d(t) = \frac{dl_d(t)}{dt} = v_{B,A}(t) + v_{A,B}(t). \qquad (37)$$

It can be calculated analytically for our LEO model using (29).

Since we do not have individual motion of the nodes, to make it a little closer to (30), we assign the range rate to the known faster moving node, as a 'pseudo node motion' scheme. All nodes' movements are included although they are used in an approximate one-end moving fashion.

For the direction A→B, the direct range is a source-moving scenario, let $v_{B,A}(t) = 0$ in (31) the received frequency at B as

$$f_{B,d}(t) = f_0/(1 + v_d(t)/c). \qquad (38)$$

For the direction B→A, it is receiver-moving and let $v_{B,A}(t) = 0$ in (32) the received frequency at A is

$$f_{A,d}(t) = f_0(1 - v_d(t)/c). \qquad (39)$$

The reflected link is treated by cascaded sections – the 's' scheme [11]. This is the same as Section 4.1 where the Doppler-shifted frequency at the reflector is deemed as a new source frequency for the next section.

Relative to A's movement, C moves much slower. This can be seen from the range rates in Fig. 4 (c) as $|v_2| \ll |v_1|$. The definition of v_1 and v_2 will follow.

Therefore, for the direction A → C, the received frequency at C is

$$f_1(t) = f_{C,A}(t) \approx f_0/(1 + v_1(t)/c) \qquad (40)$$

where

$$v_1(t) = \frac{dl_1(t)}{dt} = v_{C,A}(t) + v_{A,C}(t). \qquad (41)$$

Compared with a fixed B, C moves faster especially at the edges of pass-overs. For the direction C→B the received frequency at B is

$$f_{B,C}(t) \approx f_{C,A}(t)/(1 + v_2(t)/c). \qquad (42)$$

Substitute $f_{C,A}(t)$ in (40) and write $f_{B,C}(t)$ as $f_{Bs,r}(t)$ for the whole reflected link.

$$f_{Bs,r}(t) = \frac{f_0}{(1 + v_1(t)/c)(1 + v_2(t)/c)}. \qquad (43)$$

where

$$v_2(t) = \frac{dl_2(t)}{dt} = v_{C,B}(t) + v_{B,C}(t). \qquad (44)$$

For path B→C→A, we first look at section B→C. Assume B is almost fixed, it is a receiver-moving scenario. When f_0 is transmitted from B, the received frequency at C is

$$f_2(t) = f_{C,B}(t) \approx f_0(1 - v_2(t)/c) \qquad (45)$$

The section along C→A is also receiver-moving as the satellite moves faster. The frequency received at A is $f_{A,C}(t) \approx f_{C,B}(t)\,(1 - v_1(t)/c)$, or

$$f_{As,r}(t) = f_0(1 - v_1(t)/c)(1 - v_2(t)/c). \qquad (46)$$

Reflected link as a whole - the 'w' scheme. It treats the two reflected link sections together. The total link length is a scalar sum, $l_r(t) = l_1(t) + l_2(t)$. Its range rate is

$$v_r(t) = \frac{dl_r(t)}{dt} = v_1(t) + v_2(t). \qquad (47)$$

This is effectively the spatial mirror method [12] as in Fig. 8. The link ACB, for example, is obtained from ACB' or A'CB using mirror images l_2' or l_1' respectively.
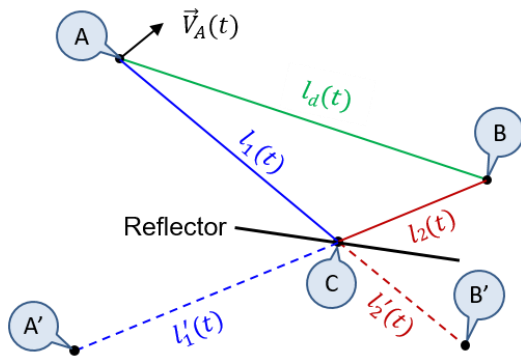

Fig. 8 – Range rate calculated using 'mirror extension' or the whole reflect link length variation – the 'w' scheme.

For the downlink the received frequency is

$$f_{Bw,r}(t) \approx \frac{f_0}{(1 + v_r(t)/c))} \qquad (48)$$

For the uplink

$$f_{Aw,r}(t) \approx f_0(1 - v_r(t)/c) \qquad (49)$$

The 'w' scheme assumes the Doppler effect is uniform along the link, in contrast to the 's' scheme. It is not justified to choose one scheme so we will implement both and compare the results numerically.

5. TWO-RAY DOPPLER CHANNEL MODELS

In this section we introduce Doppler effects to the two-ray model. To keep it accurate we try to use analytical methods as far as possible and a numerical approach when needed. A pure numerical simulation is impractical due to the excessive number of samples. As the system is time-variant some special treatment will be applied.

5.1 An analytical model

A two-ray Doppler channel model is represented by its CW response. Assume the transmitted signal is

$$s_{TX}(t) = e^{i2\pi f_0 t} \qquad (50)$$

The received signal is

$$s_{RX}(t) = V_d(t)e^{i\varphi_d(t)} + V_r(t)e^{i\varphi_r(t)} \qquad (51)$$

The two terms represent the direct ray and the reflected ray. The $\varphi_d(t)$ and $\varphi_r(t)$ are generalized phases with carrier components $2\pi f_d t$ and $2\pi f_r t$ in them, respectively. The direct ray's amplitude is

$$V_d(t) = \frac{c g_1(0) g_2(\vartheta_d)}{4\pi f_d(t) l_d(t)} \qquad (52)$$

where $f_d(t)$ is the carrier after Doppler shift for the direct ray. The reflected ray's amplitude is

$$V_r = \frac{c|\rho| g_1(\psi_1) g_2(\vartheta_r)}{4\pi f_r(t) l_r(t)} \qquad (53)$$

where $f_r(t)$ is the carrier frequency after Doppler for the reflected ray, which may be different for each direction. $l_r(t) = l_1(t) + l_2(t)$ is the length of the reflected ray. As the reflection coefficient is complex, $\rho = |\rho| \exp i\varphi_\rho$, only the amplitude is used here. The phase φ_ρ will be added to the phase of the received signal. The values $|\rho_h|$ and $\varphi_{\rho h}$ are given in (15) and $|\rho_v|$ and $\varphi_{\rho v}$ given in (17) for horizontal polarization and vertical polarization respectively.

The channel's CW response or complex gain is

$$G = \frac{s_{RX}(t)}{s_{TX}(t)} = V_d e^{i\Phi_d(t)} + V_r e^{i\Phi_r(t)} \qquad (54)$$

where $\Phi_d(t) = \varphi_d(t) - 2\pi f_0 t$ and $\Phi_r(t) = \varphi_r(t) - 2\pi f_0 t$ are the baseband phase responses. If we have it referenced on the direct ray, we have the tilted phase CW response

$$G' = \frac{G}{e^{i\Phi_d(t)}} = V_d + V_r e^{i\Phi'(t)} \qquad (55)$$

where the tilted phase is
$$\begin{aligned}\Phi'(t) &= \Phi_r(t) - \Phi_d(t) \\ &= \varphi_r(t) - \varphi_d(t)\end{aligned} \qquad (56)$$

Our task now is calculating $\varphi_r(t)$ and $\varphi_d(t)$.

The phase of a signal after each link consists of a carrier term and a phase shift term due to the path delay difference. Unlike the static case, the time-varying carriers, $2\pi f_r(t)t$ and $2\pi f_d(t)t$, cannot be cancelled as the frequencies are different. There will be a 'beat effect' when combined. Also, the phase shift due to delay is not a simple product (unless using approximations) but an integration, as both the frequency and the link length are time varying.

For the direct link the phase of the received signal is

$$\varphi_d(t) = 2\pi f_d(t)t + 2\pi \int_{t-\frac{l_d(t)}{c}}^{t} f_d(\tau)\, d\tau \qquad (57)$$

The integration period $l_d(t)/c$ is the duration the signal travels along $l_d(t)$ at time t.

With the Doppler shift expressions given in the last section, the integral (57) is solvable only for the receiver-moving (uplink) case. When substituting (39) in (57) the phase is

$$\begin{aligned}\varphi_{A,d}(t) &= 2\pi f_{A,d}(t)t \\ &\quad + 2\pi \int_{t-\frac{l_d(t)}{c}}^{t} f_{A,d}(\tau)\, d\tau \\ &= 2\pi f_{A,d}(t)t \\ &\quad + 2\pi \int_{t-\frac{l_d(t)}{c}}^{t} f_0(1 - v_d(\tau)/c)\, d\tau\end{aligned} \qquad (58)$$

Considering $v_d(t) = dl_d(t)/dt$ (37) the integral is

$$\begin{aligned}\varphi_{A,d}(t) &= 2\pi f_{A,d}(t)t \\ &\quad + 2\pi \frac{f_0}{c} l_d(t - l_d(t)/c)\end{aligned} \qquad (59)$$

Note in (59) the bracket after l_d denotes the function relationship, not a product. That is, $l_d(t - \frac{l_d(t)}{c})$ is the length of the direct path at time $t - \frac{l_d(t)}{c}$. To calculate this length precisely, we go back in time from t by $\frac{l_d(t)}{c}$. Further discussion is in Section 5.3.

For the reflected link, only for the uplink 'w' scheme, the integral is solvable. The signal phase is

$$\begin{aligned}\varphi_r(t) &= 2\pi f_r(t)t + 2\pi \int_{t-\frac{l_r(t)}{c}}^{t} f_r(\tau)\, d\tau \\ &\quad + \varphi_\rho\end{aligned} \qquad (60)$$

When substituting (49) into (60) we have

$$\begin{aligned}\varphi_{Aw,r}(t) &= 2\pi f_{Aw,r}(t)t + \varphi_\rho(f_{Aw,r}) \\ &\quad + 2\pi \int_{t-\frac{l_r(t)}{c}}^{t} f_{Aw,r}(\tau)\, d\tau \\ &= 2\pi f_{Aw,r}(t)t + \varphi_\rho(f_{Aw,r}) \\ &\quad + 2\pi \int_{t-\frac{l_r(t)}{c}}^{t} f_0(1 - v_r(t)/c)\, d\tau\end{aligned} \qquad (61)$$

Considering $v_r(t) = \frac{dl_r(t)}{dt}$ as given in (47), we have

$$\begin{aligned}\varphi_{Aw,r}(t) &= 2\pi f_{Aw,r}(t)t + \varphi_\rho(f_{Aw,r}) + \\ &\quad 2\pi \frac{f_0}{c} l_r(t - l_r(t)/c)\end{aligned} \qquad (62)$$

Again, $l_r(t - l_r(t)/c)$ is the length of the reflected path at time $t - l_r(t)/c$.

For the uplink, the phase response can be obtained as

$$\Phi'_{Aw}(t) = \varphi_{Aw,r}(t) - \varphi_{A,d}(t) \qquad (63)$$

When substituting (62) and (58) we have

$$\begin{aligned}\Phi'_{Aw}(t) &= 2\pi(f_{Aw,r}(t) - f_{A,d}(t))t \\ &\quad + 2\pi \frac{f_0}{c}(l_r(t - l_r(t)/c) \\ &\quad - l_d(t - l_d(t)/c)) + \varphi_\rho(f_{Aw,r})\end{aligned} \qquad (64)$$

Note the brackets after l_r and l_d denote the function relationships with time. This is the only analytical solution. If $f_{Aw,r}(t)$ can also be calculated analytically then it is accurate. Unfortunately, this is not the case, although its influence is minor. See Section 5.3.1 for more discussions. For all downlink and sectional Doppler treatment of the reflected path ('s' schemes), the integrals are not solvable, and approximations must be used.

5.2 Piecewise time-invariant approximations

In the integrals in (57) and (60), both frequency and path lengths are time variant. If we treat the velocities and link lengths as constants at a given time, we obtain the piece-wise Time-Invariant (TI) approximations.

For the downlink A→B the phase is

$$\varphi_{B,d}(t) = 2\pi f_{B,d}(t)t + 2\pi \int_{t-\frac{l_d(t)}{c}}^{t} f_{B,d}(\tau)\, d\tau \quad (65)$$

Substitute the Doppler expressions $f_{B,d}$ of (38) and assuming $v_d(t)$ is a constant during the integration period, we have $\varphi_{B,d}(t) \approx \varphi_{B,d,TI}(t)$ and

$$\varphi_{B,d,TI}(t) = 2\pi f_{B,d}(t)t + 2\pi \frac{f_0 l_d(t)}{c(1+v_d(t)/c)} \quad (66)$$

For the uplink the accurate solution was derived in (59). The TI approximation may still be useful for comparison. From (58), treating $v_d(t)$ as time invariant we obtain

$$\varphi_{A,d,TI}(t) = 2\pi f_{A,d}(t)t + 2\pi \frac{f_0 l_d(t)}{c}\left(1 - \frac{v_d(t)}{c}\right) \quad (67)$$

For the reflected down link, if it is treated as a whole ('w' scheme), the phases can be calculated similarly. The received phase at B is

$$\begin{aligned}\varphi_{Bw,r}(t) &= 2\pi f_{Bw,r}(t)t + \varphi_\rho(f_{Bw,r}) \\ &\quad + 2\pi \int_{t-\frac{l_r(t)}{c}}^{t} f_{B,r}(\tau)\, d\tau \\ &\approx \varphi_{Bw,r,TI} = 2\pi f_{Bw,r}(t)t + \varphi_\rho(f_{Bw,r}) \\ &\quad + 2\pi \frac{f_0 l_r(t)}{c(1+v_r(t)/c)}\end{aligned} \quad (68)$$

For the reflected uplink, apart from the analytical expression (62), its TI approximation is

$$\begin{aligned}\varphi_{Aw,r,TI}(t) &= 2\pi f_{Aw,r}(t)t + \varphi_\rho(f_{Aw,r}) \\ &\quad + 2\pi \frac{f_0 l_r(t)}{c}(1 - v_r(t)/c)\end{aligned} \quad (69)$$

If the Doppler in the reflected path is treated section by section ('s' scheme), the TI phases can be derived accordingly. For the downlink,

$$\begin{aligned}\varphi_{Bs,r}(t) &= 2\pi f_{Bs,r}(t)\,t + \varphi_\rho(f_1) \\ &\quad + 2\pi \int_{t-\frac{l_r(t)}{c})}^{t-l_2(t)/c} f_1(\tau)\, d\tau \\ &\quad + 2\pi \int_{t-l_2(t)/c}^{t} f_{Bs,r}(\tau)\, d\tau\end{aligned} \quad (70)$$

Substitute $f_1(\tau)$ according to (40) and $f_{Bs,r}(\tau)$ in (43), and treating $v_1(t)$ and $v_2(t)$ as time invariant we have $\varphi_{Bs,r}(t) \approx \varphi_{Bs,r,TI}(t)$ and

$$\begin{aligned}\varphi_{Bs,r,TI}(t) &= 2\pi f_{Bs,r}(t)\,t + \frac{2\pi f_0 l_1(t)/c}{1+v_1(t)/c} \\ &\quad + \frac{2\pi f_0 l_2(t)/c}{(1+v_1(t)/c)(1+v_2(t)/c)} + \varphi_\rho(f_1)\end{aligned} \quad (71)$$

Note here we have used $l_r(t) - l_2(t) = l_1(t)$.

For the uplink, we have

$$\begin{aligned}\varphi_{As,r}(t) &= 2\pi f_{As,r}(t)\,t + \varphi_\rho(f_2) \\ &\quad + 2\pi \int_{t-\frac{l_r(t)}{c})}^{t-l_1(t)/c} f_2(\tau)\, d\tau \\ &\quad + 2\pi \int_{t-l_1(t)/c}^{t} f_{As,r}(\tau)\, d\tau\end{aligned} \quad (72)$$

When substituting $f_2(\tau)$ according to (45) and $f_{As,r}(\tau)$ in (46) and integrate it, we have $\varphi_{As,r}(t) \approx \varphi_{As,r,TI}(t)$ and

$$\begin{aligned}\varphi_{As,r,TI}(t) &= 2\pi f_{As,r}(t)t + \varphi_\rho(f_2) \\ &\quad + 2\pi \frac{f_0 l_2(t)}{c}(1 - v_2(t)/c) \\ &\quad + 2\pi (f_0 l_1(t)/c)(1-v_1(t)/c)(1-v_2(t)/c)\end{aligned} \quad (73)$$

To simplify the notations next, some intermediate factors are introduced in Table 1.

Table 1 – Intermediate factors

$N_1 = 1 - v_1(t)/c$	$Q_1 = 1/(1+v_1(t)/c)$
$N_2 = 1 - v_2(t)/c$	$Q_2 = 1/(1+v_2(t)/c)$
$N_d = 1 - v_d(t)/c$	$Q_d = 1/(1+v_d(t)/c)$
$N_r = 1 - v_r(t)/c$	$Q_r = 1/(1+v_r(t)/c)$

The phase responses are phase differences between the reflected signal and the direct signal. For the 'w' downlink $\Phi'_{Bw}(t) = \varphi_{Bw,r}(t) - \varphi_{B,d}(t)$. From (68) and (66), as well as (48) and (38) and Table 1, we have the TI phase response

$$\begin{aligned}\Phi'_{Bw,TI}(t) &= 2\pi f_0((Q_r - Q_d)t \\ &\quad + (l_r(t)Q_r - l_d(t)Q_d)/c) + \varphi_\rho(f_{Bw,r})\end{aligned} \quad (74)$$

Similarly, for the uplink, $\Phi'_{Aw,TI}(t) = \varphi_{Aw,r,TI}(t) - \varphi_{A,d,TI}(t)$. From (69), (67), (49), (39) and Table 1,

$$\begin{aligned}\Phi'_{Aw,TI}(t) &= 2\pi f_0((N_r - N_d)t \\ &\quad + (l_r(t)N_r - l_d(t)N_d)/c) + \varphi_\rho(f_{Aw,r})\end{aligned} \quad (75)$$

For the downlink, $\Phi'_{Bs,TI}(t) = \varphi_{Bs,r,TI}(t) - \varphi_{B,d,TI}(t)$. From (71), (66), (43), (38) and Table 1,

$$\Phi'_{Bs,TI}(t) = 2\pi f_0((Q_1 Q_2 - Q_d)t \\ + (l_1(t)Q_1 + l_2(t)Q_1 Q_2 \quad (76) \\ - l_d(t)Q_d)/c) + \varphi_\rho(f_1)$$

For the uplink, from (73), (67), (46), (39) and Table 1,

$$\Phi'_{As,TI}(t) = 2\pi f_0((N_1 N_2 - N_d)t \\ + (l_2(t)N_2 + l_1(t)N_1 N_2 \quad (77) \\ - l_d(t)N_d)/c) + \varphi_\rho(f_2)$$

For different schemes and directions, the channel gains are

$$G'_x(dB) = 20 \log_{10} |G_x'| \quad (78)$$

where x is the code of scheme including algorithm and direction. The code names will be discussed in Section 5.4.

Note when using $\varphi_\rho(f_0)$ in places of $\varphi_\rho(f_x)$ for a few different schemes, there is no obvious difference as shown in numerical results. We still use individual frequencies for accuracy.

5.3 Numerical computation

5.3.1 An irregular sampling method

In the analytical calculation of (64), the two range lengths $l_d(t - l_d(t)/c)$ and $l_r(t - l_r(t)/c)$ need to be calculated at time $t - l_d(t)/c$ and $t - l_r(t)/c$ respectively. It means $l_d(t)$ and $l_r(t)$ must be calculated first at time t, and then go back in time by $T_d(t) \triangleq l_d(t)/c$ and $T_r(t) \triangleq l_r(t)/c$, to calculate the required range lengths. $T_d(t)$ and $T_r(t)$ are the times the waves travel on $l_d(t)$ and $l_r(t)$ respectively. Since $T_d(t)$ and $T_r(t)$ vary with time this is an Irregular Sampling (IS) system. Fortunately, our satellite pass-over model allows for this.

The sampling relationship is plotted in Fig. 9. Sampling happens first at regular instances T_s apart, where T_s is the main sampling period.
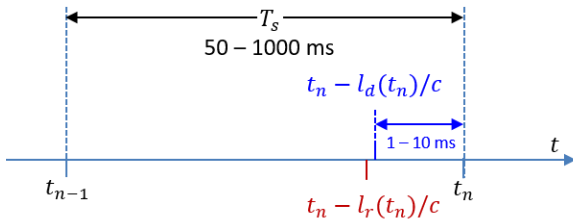
Fig. 9 – Irregular sampling relationship, not drawn to scale.

The simulation is performed in several steps. First, it runs in regular sampling intervals at

$$t_n = nT_s, n = 1, 2, \cdots M \quad (79)$$

to obtain relevant range lengths, where M is the total number of samples in the pass-over. The direct range length is calculated precisely using (22)

$$l_{d,n} = l_d(t_n) = l_d(nT_s), n = 1, 2, \cdots M \quad (80)$$

With the solver we calculate $l_{1,n} = l_1(t_n)$ and $l_{2,n} = l_2(t_n)$ and sum up to obtain the reflected range length

$$l_{r,n} = l_r(t_n) = l_r(nT_s), n = 1, 2, \cdots M \quad (81)$$

Then we go back and set the sampling instances according to $T_d(t_n) = l_{d,n}/c$ and $T_r(t_n) = l_{r,n}/c$ respectively at

$$t_{n,d} = t_n - T_d(t_n), n = 1, 2, \cdots M \quad (82)$$

and

$$t_{n,r} = t_n - T_r(t_n), n = 1, 2, \cdots M \quad (83)$$

The direct link length at the time $t_{n,d}$ is calculated as

$$l_{d,n,d} = l_d(t_{n,d}), n = 1, 2, \cdots M \quad (84)$$

The direct link length at the time $t_{n,r}$ is calculated as

$$l_{d,n,r} = l_d(t_{n,r}), n = 1, 2, \cdots M \quad (85)$$

The last letter 'd' or 'r' in the subscripts indicates the offset time being associated with $T_d(t)$ or $T_r(t)$ respectively.

The reflected link can be calculated from $l_{d,n,r}$. First solve (5) for the reflected link sections

$$l_{1,n,r} = l_1(t_{n,r}), n = 1, 2, \cdots M \\ l_{2,n,r} = l_2(t_{n,r}), n = 1, 2, \cdots M \quad (86)$$

Then sum up to obtain

$$l_{r,n,r} = l_r(t_{n,r}) = l_{1,n,r} + l_{2,n,r}, \\ n = 1, 2, \cdots M \quad (87)$$

Here we have implemented a time-varying sampling system. At different times we have different time offset $T_d(t_n)$ and $T_r(t_n)$ from the regular sampling instances t_n. All required geometry and motion parameters are re-calculated at the new instances starting from the new values of longitudes $\xi(t_{n,d})$ and $\xi(t_{n,r})$ using (20).

The Irregular Sampled (IS) uplink tilted phase is

$$\Phi'_{Aw,IS}(t_n) = 2\pi(f_{Aw,r}(t_n) \\ - f_{A,d}(t_n))t_n \\ + 2\pi \frac{f_0}{c}(l_{r,n,r} - l_{d,n,d}) \quad (88) \\ + \varphi_\rho(f_{Aw,r})$$

Note it is not fully analytical, as in the computation of $f_{Aw,r}$ with (49) the $v_r(t)$ is still obtained numerically. In the computation of $f_{A,d}$ although $v_d(t)$ can be obtained analytically, practically it is still calculated numerically for consistency with $v_r(t)$.

5.3.2 A double sampling method

The computation of TI approximations (Section 5.2) requires further elaboration.

First, we determine the sampling interval T_s. When $f_0 \geq 10$ GHz and $h_2 \geq 10$ m, the channel fades relatively fast. The channel gain may be sufficiently represented by a sampling period of $T_s = 50$ ms. For this sample rate there are up to 20000 samples during a pass-over. Using the high precision arithmetic MATLAB *vpa,* the execution time is many hours on a standard PC. To reduce the run time, we use longer sampling intervals, e.g. $T_s = 1$ second when f_0 and h_2 are lower.

On the other hand, the propagation delay, e.g. for the range l_d/c is far less than the sampling interval, $l_d/c \ll T_s$, as illustrated in Fig. 9. It is 1 ms $\leq l_d/c \leq$ 10 ms for the range of 300 km $\leq l_d \leq$ 3000 km. To perform numerical integration by cumulative sum is impossible, as there are no multiple samples to use. Also, the velocity calculation is inaccurate using the long T_s steps due to time varying.

To overcome these problems, we used a double-sample method for the TI calculations, as shown in Fig. 10. A small time-chip $1 \leq T_C \leq 5$ ms is added to each regular sample to form a second sampling serial. The range lengths are now calculated at T_C steps for the related velocity $v \approx \Delta l/T_C$.
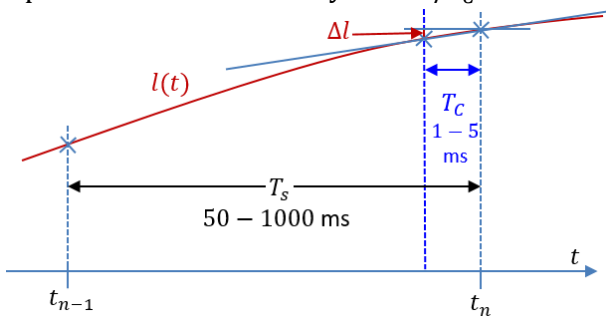
Fig. 10 – Difference operation at the t_n vicinity using the sample at $t_n - T_C$ instead of t_{n-1}. Not drawn to scale.

Fig. 11 plots the absolute values of calculated range rate v_d from (29), and errors from three numerical methods. Among them the one using step $T_s = 1$ s has the largest error. The error using $T_C = 2$ ms is much smaller, as expected. The IS offers the smallest error.
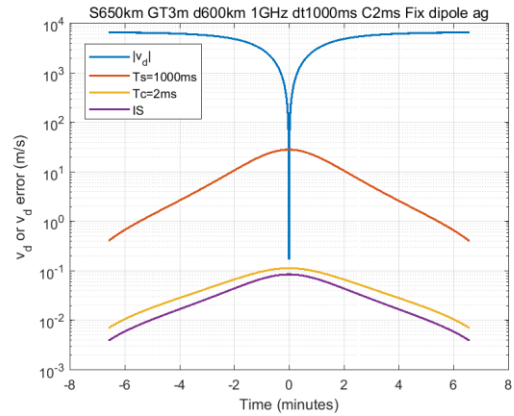

Fig. 11 – Example of direct link range rate $|v_d(t)|$ and errors from different numerical methods, $T_s = 1$ s and $T_C = 2$ ms.

Mixed calculations using (29) and numerical method may produce unexpected errors, so that for the TI schemes both $v_d(t)$ and $v_r(t)$ should be calculated numerically, as there is no formula for the latter.

5.4 Scheme codes

We have configured 13 schemes for comparison. The codes of two-Ray Doppler (2RD) schemes are named as follows. The first letter 'A' or 'B' represents the receive end of a link, i.e. 'A' for an uplink, and 'B' for a downlink. The next letter, 'w' for the Doppler based on the whole reflected path, and 's' for sectional Doppler. Then it is 'h' or 'v' for horizontal and vertical polarization respectively. There are only two schemes obtained by irregular sampling 'IS', namely 'AwhIS' and 'AwvIS'. The rest are Time-Invariant (TI) approximates, where 'TI' may be omitted. For the uplink, these 2RD schemes are 'Ash', 'Asv', 'Awh', 'Awv'. For the downlink, they are 'Bsh', 'Bsv', 'Bwh', 'Bwv'. There are also the static two-ray model '2Rh' and '2Rv', and the LOS model.

6. NUMERICAL EXAMPLES AND DISCUSSIONS

In this section we present some numerical results along with comparisons and discussions.

6.1 Doppler shift difference

The speculated non-zero Doppler shift differences between the two rays, are plotted in Fig. 12 , using the 'Aw' as examples. For the same SAT-GT system (h_1, d) , the Doppler difference increases with ground antenna height h_2 and frequency f_0.
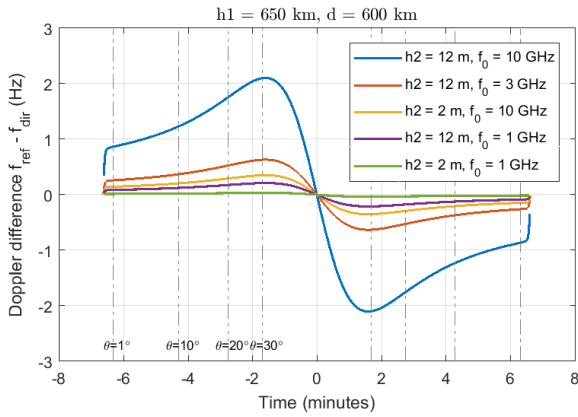
Fig. 12 – Doppler shift difference between two rays, given ground antenna height and carrier frequency, 'Aw', conditions in top title.

6.2 Comparison of schemes

Comparison of the results from different schemes and conditions may help check the algorithms and raise confidence in the models. The following comparisons will be considered. (1) IS versus TI; (2) 's' vs 'w'; (3) Uplink 'A' vs downlink 'B'; and (4) 'h' vs 'v' polarization. Different h_1 and d will also be used throughout this section.

An example is given in Fig. 13. The analytical scheme $\Phi'_{Aw,IS}(t)$ using (88) has virtually an identical result with the TI approximation $\Phi'_{Aw,TI}(t)$ using (75).
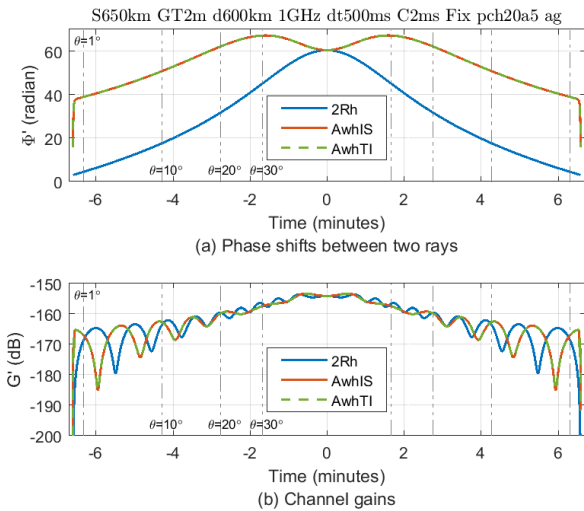
Fig. 13 – Phase and gain plots for two-ray static (2Rh) and some two-ray Doppler models. The uplink irregular sampling ('AwhIS'), and time-invariant approximation ('AwhTI') have little difference.

In most plots the conditions are given in the top title. In Fig. 13, $T_C = 2$ ms is used for $\Phi'_{Aw,TI}(t)$, as well as v_r and v_d calculations for $f_{Aw,r}$ and $f_{A,d}$ used in $\Phi'_{Aw,IS}(t)$. The SAT height $h_1 = 650$ km, GT height $h_2 = 2$ m and $d = 600$ km from GT to the sub-SAT track, $f_0 = 1$ GHz, a -20 dB back gain patch antenna is used, with an average ground.

Some phase differences are plotted in Fig. 14. The difference between uplink IS and TI schemes is very small as shown in Fig. 14 (a).

The uplink and downlink phase have a noticeable difference between source-moving and receiver-moving models. An example is shown in Fig. 14 (b). With $f_0 = 1$ GHz and $h_2 = 2$ m, the maximum phase difference is under 0.1°. If $f_0 = 30$ GHz it will rise to 2.5°. This small phase difference will not cause significant change in channel gain. The uplink and downlink gain curves are virtually identical.
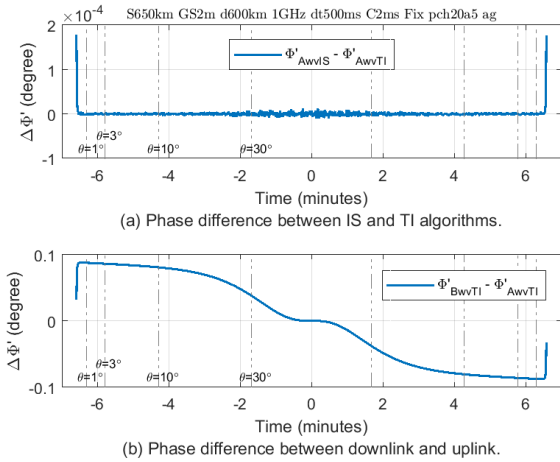

Fig. 14 – Phase differences, between two algorithms (a), and between the downlink and uplink (b), vertical polarization.

A comparison of 's' schemes 'Ash' and 'Bsh' with 'w' scheme 'Awh' is shown in Fig. 15. They agree well except when $\theta \leq 1°$.

The phases of 's' and 'w' schemes only diverge at the ends of a pass-over. For the most used elevation angles they agree well. This helps confirm our models are likely to be correct there. Further comparisons of the schemes will follow in another context.
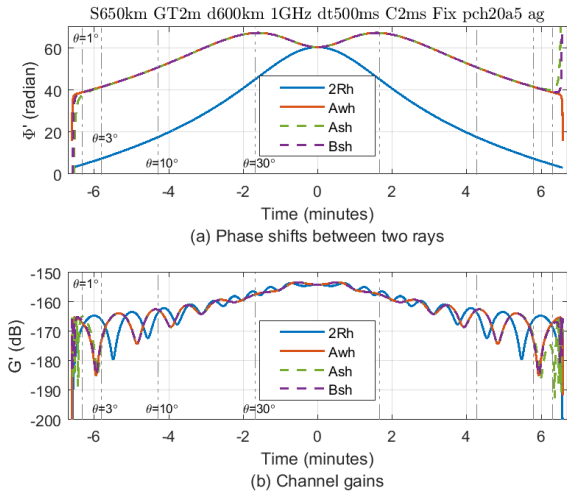
Fig. 15 – Example of phase and channel gains for 'Awh', 'Ash' and 'Bsh' schemes. For 'Ash' and 'Bsh' the phase start to diverge when $\theta \le 3°$. Rapid fading happens when $\theta \le 1°$ for 'Ash', $\theta \le 0.5°$ for 'Bsh'.

6.3   Ground antenna radiation pattern

The ground antenna radiation pattern plays a key role in the two-ray responses. As per Fig. 5 (b) there is a significant difference between the viewing angles of the two rays. A good antenna should reject the ground reflection as much as possible.

To demonstrate this effect, we use several antennas, including a practical helical antenna, an artificial patch antenna family, idealized horizontal and vertical dipoles, and the omnidirectional antenna.

6.3.1 Helical antenna

A real tracking 18.5 dBi helical antenna is tested first. Its linear voltage radiation is plotted in Fig. 16. Some channel gains are plotted in Fig. 17 for a GT to sub-SAT track distance $d = 800$ km scenario.
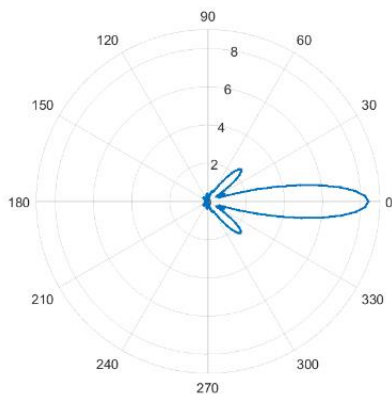
Fig. 16 – A helical antenna pattern in linear scale versus ϑ.
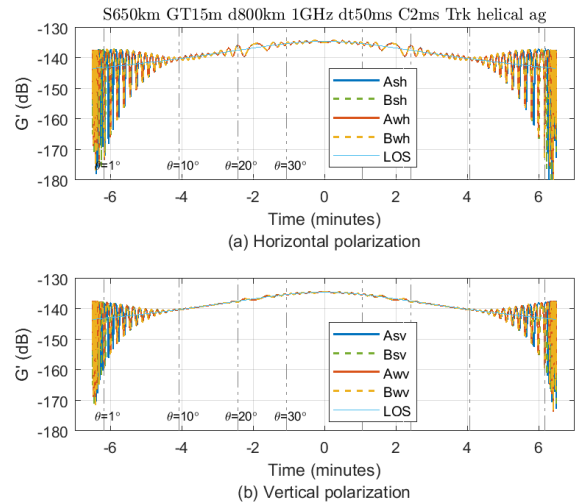
Fig. 17 – Tracking helical antenna selected channel gains.

The elevation-wise selectivity and the tracking made the channel response free from deep fading when the elevation angle $\theta > 10°$. All schemes agree well in this commonly working elevation region.

We take this example to observe the different schemes at low elevation angles. The ends' details of Fig. 17 (a) are plotted in Fig. 18.
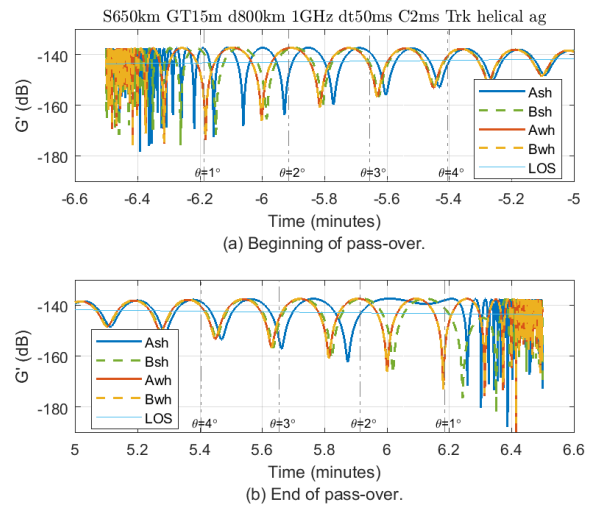

Fig. 18 – Details of Fig. 17 (a) at low elevation regions, 'Ash' has longer high frequency fading periods than others. 'Awh' and 'Bwh' are almost identical.

The schemes are almost the same when $\theta > 4°$. All have a dense fading period when $\theta < 0.5°$ at both ends of a pass-over. The uplink 'Awh' and downlink 'Bwh' spatial mirror Doppler schemes are near identical for the whole pass-over. The 's' schemes stand out with the 'Ash' more prominent. The very dense fading period is longer for 'Awh'. The trend is similar for vertical polarized responses.

The agreements for all schemes when $\theta > 10°$ serve as cross-checks and validations for the schemes.

Note that at the very edge the sampling rate is insufficient for the very fast fading, hence not able to reflect the full fading depth.

6.3.2 Patch antennas

We artificially generated a family of patch antenna patterns with different back gains. They are specified by two parameters g_n and a. g_n is the back voltage gain. For example, $g_n = 0.1$, $G_n = 20 \log_{10} g_n = -20$ dB. $a \in (0,1)$ is a small constant that helps to produce a non-zero gain at zero elevation. The voltage gain is calculated by

$$g_a = \begin{cases} g_p = \dfrac{a + \sin\theta}{1 + a}, & \text{if } g_p \geq g_n \\ g_n, & \text{otherwise} \end{cases} \quad (89)$$

In Fig. 19 three patterns are plotted.
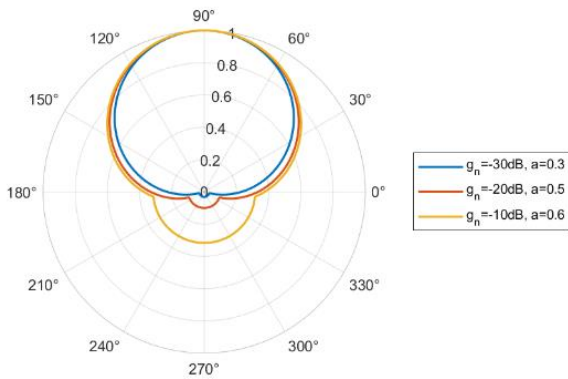
Fig. 19 – Artificial patch radiation patterns.

The maximum gain of the patch is upwards, assuming it is deployed as a fixed antenna. The channel gains of three antennas are plotted in Fig. 20. The deep fading even at high elevation angles corresponds to the poor antenna in (a) and fades less with a better antenna (c).
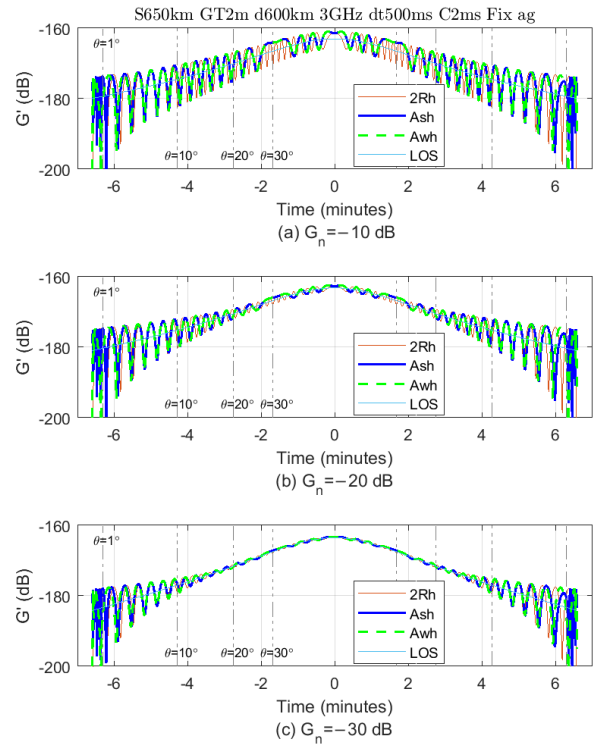

Fig. 20 – Response for artificial patch antennas, with back gain $G_n = -10$ dB, -20 dB and -30 dB, $h_2 = 2$ m, $f_0 = 3$ GHz.

6.3.3 Omnidirectional antenna

A hypothetical omnidirectional antenna along the elevation angle is used, as in Fig. 21. The two-ray interference fading is among the worst over the pass-over, as shown in Fig. 22.
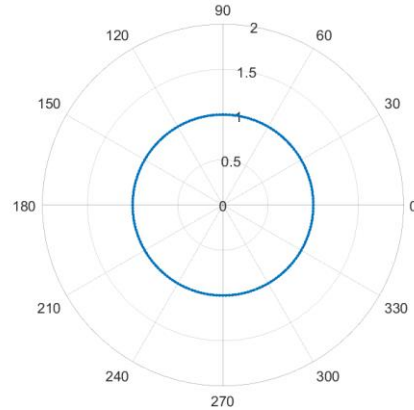
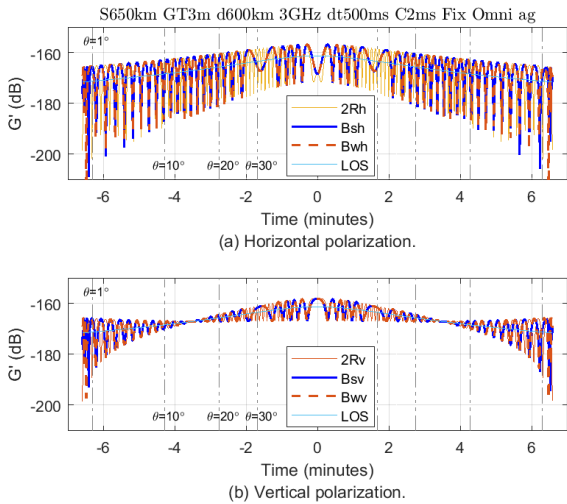

Fig. 21 – Omnidirectional radiation pattern.

Fig. 22 – Channel gains using omnidirectional antenna. Fading in horizontal polarization is larger than vertical polarization, $d = 600$ km, $h_2 = 3$ m, $f_0 = 3$ GHz.

6.3.4 Dipole antenna

Vertical monopole and dipole antennas are used extensively for VHF and UHF radios. It is interesting to see how they behave with a two-ray LEO channel. For this purpose, we generated an artificial 'doughnut' shaped dipole pattern, as in Fig. 23.
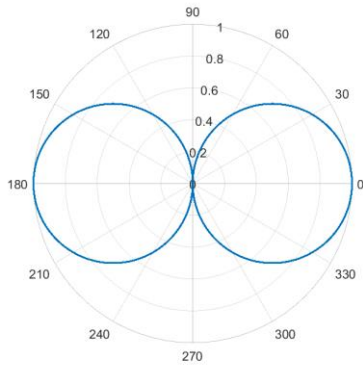

Fig. 23 – The linear radiation pattern of an artificial vertical dipole antenna.

A channel gain example is plotted in Fig. 24 for a high elevation pass-over, with $d = 150$ km. The highest elevation is $\theta = 75.7°$. As expected, there is a valley in the middle of the pass-over due to the lower antenna gains there. For lower elevation pass-overs the responses are like omnidirectional ones.
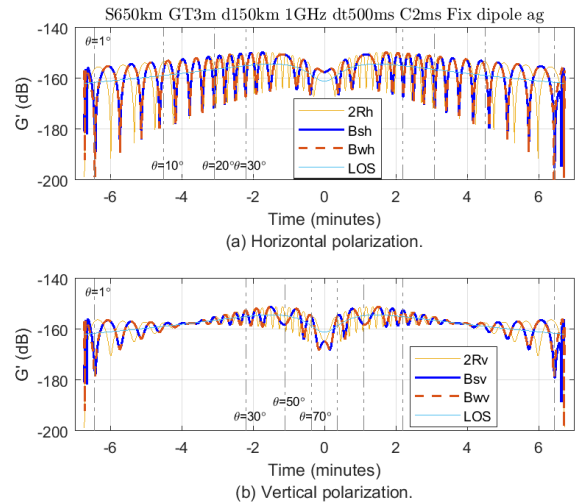

Fig. 24 – Channel gains for a vertical dipole antenna, $d = 200$ km, $h_2 = 3$ m, $f_0 = 1$ GHz.

6.4 Carrier frequency

For a same set of conditions, the fading rate is proportional to the carrier frequency. This is plotted in Fig. 25 for 400 MHz, 2 GHz and 10 GHz respectively using a $G_n = -20$ dB artificial patch antenna.
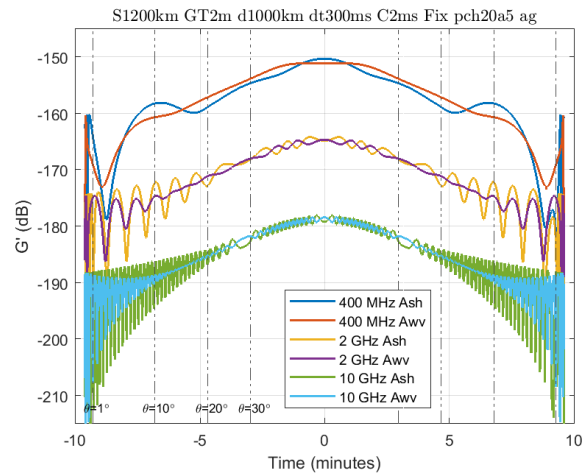

Fig. 25 – Three frequencies and two polarizations, satellite height $h_1 = 1200$ km, GT height $h_2 = 2$ m, -20 dB patch antenna.

6.5 Ground antenna height

The ground antenna height plays a similar role to the carrier frequency. The higher it is, the more frequently the amplitude fluctuates. Examples are plotted in Fig. 26, for $h_2 = 2$ m, 5 m and 12 m.

From Fig. 26 we can also see that the uplink 'Awv' and downlink 'Bwv' responses are almost identical.
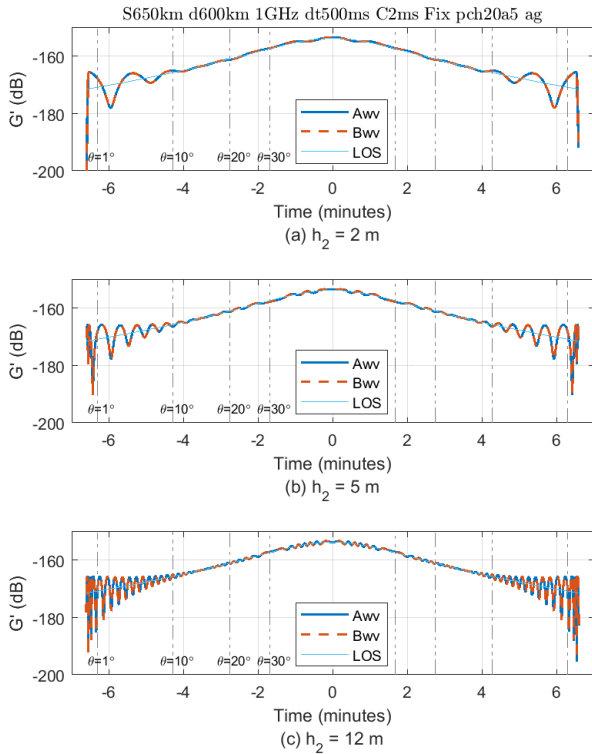
Fig. 26 – Ground antenna heights, h_2 = 2 m, 5 m, and 12 m, 1 GHz, 'Awv' versus 'Bwv' with no observable difference.

7. CONCLUSIONS

In this paper we presented some two-ray models for LEO satellite links. They include the effects of ground reflection and Doppler effects due to satellite movement.

Based on a satellite pass-over, the Doppler shift difference between the two rays was calculated with several range rate-based Doppler models and approximations. Analytical and numerical algorithms were constructed for the channel's CW responses.

With Doppler effects the channel loss changes with a frequency beat component on top of the classic two-ray phase shift. The fading periods become irregular while the envelope is almost unchanged from the static two-ray model.

More importantly, the increased fidelity of the models raises confidence in applying the two-ray model to LEO scenarios without the concern that the motion factor was not counted in. Traditionally a two-ray channel is for stationary or slow-moving radios.

With the two-ray Doppler models we verified that our high gain tracking antenna works very well as expected. Fixed up-facing patch antennas offer reasonable performance due to their low backside gains. We also showed that the omnidirectional and dipole antennas have poor performance. We observed that the fading rate increases with the ground antenna height and carrier frequency.

By comparing the numerical results, we are pleased to see that the difference between our Doppler models is insignificant for normally used elevation angles, usually $\theta > 10°$. They diverge only at very low elevation angles. The largest difference is between the sectional Doppler ('s' scheme) and the spatial mirror Doppler ('w' scheme), especially the uplink 'As'. It happens, for example, when $\theta < 4°$ or even when $\theta < 1°$. The uplink and downlink spatial mirror schemes 'Aw' and 'Bw' are almost identical. The Time-Invariant (TI) approximation results agree very well with the Irregular Sampled (IS) analytical algorithm.

That all our schemes agree well in normally used elevations is significant. It serves as a cross-check and validation before experiment data is available.

If one model is to be recommended, the spatial mirror method based 'Aw' is perhaps a good one, based on its simplicity.

ACKNOWLEDGEMENT

REFERENCES

[1] G. E. Corazza and F. Vatalaro, "A statistical model for land mobile satellite channels and its application to nongeostationary orbit systems," *IEEE Trans on vehicular technology,* vol. 43, no. 3, pp. 738-742, 1994.

[2] J. M. Gongora-Torres, C. Vargas-Rosales, A. Aragon-Zavala and R. Villalpando-Hernandez, "Elevation Angle Characterization for LEO Satellites: First and Second Order Statistics," *MDPI,* vol. Appl Sci 13(7), no. 4405, 2023.

[3] M. Tropea and F. A. De Rango, "Comprehensive Review of Channel Modeling for Land Mobile Satellite Communications," *Electronics,* vol. 5, no. 11, 2022.

[4] R. H. Clarke, "A statistical theory of mobile-radio reception," *Bell Syst. Tech. Journal,* vol. 47, no. 6, p. 957–1000, July 1968.

[5] Z. Yun and M. F. Iskander, "Ray Tracing for Radio Propagation Modelling: Principles and Applications," *IEEE Access,* vol. 3, pp. 1089-1100, 2015.

[6] T. S. Rappaport, Wireless Communications: Principles and Practice, 2nd ed., Prentice Hall, 2001.

[7] A. Saakian, Radio wave propagation fundamentals, Norwood: Artech House, 2011.

[8] N. Ranchagoda, K. Sithamparanathan, M. Ding, A. Al-Hourani and K. Gomez, "Elevation-angle based two-ray path loss model for Air-to-Ground wireless channels," *Elsevier Vehicular communications,* vol. 32, pp. 1-12, December 2021.

[9] W. Hubert, Y.-M. Le Roux, M. Ney and A. Flamand, "mpact of Ship Motions on Maritime Radio Links," *Hindawi Publishing Corporation International Journal of Antennas and Propagation,* 2012.

[10] International Telecommunication Union, "Recommendation ITU-R P.527-6," 2021.

[11] Floris, "How to calculate the Doppler effect on a wave reflection when both the source and the listener are moving," Physics Stack Exchange, 23 May 2017. [Online]. Available: https://physics.stackexchange.com/questions /334933/how-to-calculate-the-doppler-effect- on-a-wave-reflection-when-both-the-source-an. [Accessed 8 April 2024].

[12] P. Zhao, X. Wang, K. Zhang, Y. Jin and G. Zheng, "Doppler Modeling and Simulation of Train-to-Train Communication in Metro Tunnel Environment," *MDPI Sensors ,* vol. 22, no. 4289, 2022.

[13] International Telecommunication Union, "Recommendation ITU-R P.2345-2 Radiowave propagation," 2020.

[14] D. E. Kerr, "Chapter 5," in *Propagation of short radio waves*, The Institution of Engineering and Technology, 1987, p. 396.

[15] B. Censor, "Theory of the Doppler effect: Fact, fiction and approximation," *Radio science,* vol. 19, pp. 1027-1040, July-August 1984.

[16] A. Guth, "The Doppler effect and special relativity," *Massachusetts Institute of technology lecture notes,* 2018.

[17] W. Liu, S. Zheng, Z. Deng, W. Ke, W. Lin, J. Lei, Y. Jin and H. Liu, "Multi-Scene Doppler Power Spectrum Modeling of LEO Satellite Channel Based on Atlas Fingerprint Method," *IEEE Access,* vol. 9, pp. 11811 - 11822, January 2021.

AUTHOR

Weimin Zhang was born in May 1953 in Jinan, China. He received his B.Eng. degree of radio engineering in 1982 from Shandong Engineering Institute. He moved to Australia in 1985 and received his Ph.D. degree in 1996 from the University of South Australia. He joined the Defence Science and Technology Organisation (later known as Defence Science and Technology Group) in 1995. He has authored and co-authored over forty conference papers, journal papers and book chapters. His research interests cover areas in wireless communications, including modulation, error control coding and channel modelling. He is a member of IEEE.